

**RESEARCH ARTICLE**

10.1029/2018JC013750

**Key Points:**

- We applied a two-particle method to produce global maps of horizontal eddy diffusivity near the surface and at 1,000 m
- Our estimated eddy diffusivities show reasonable agreement with previous studies
- We tested a mixing globalization including mixing by mean flow and obtained agreement with our estimates of diffusivity

**Supporting Information:**

- Supporting Information S1
- Figure S1

**Correspondence to:**

C. J. Roach,  
christopher.roach@utas.edu.au

**Citation:**

Roach, C. J., Balwada, D., & Speer, K. (2018). Global observations of horizontal mixing from Argo float and surface drifter trajectories. *Journal of Geophysical Research: Oceans*, 123, 4560–4575. <https://doi.org/10.1029/2018JC013750>

Received 3 JAN 2018

Accepted 30 MAY 2018

Accepted article online 8 JUN 2018

Published online 2 JUL 2018

# Global Observations of Horizontal Mixing from Argo Float and Surface Drifter Trajectories

Christopher J. Roach<sup>1</sup> , Dhruv Balwada<sup>2</sup> , and Kevin Speer<sup>3</sup>

<sup>1</sup>Institute for Marine and Antarctic Studies and ARC Centre of Excellence for Climate System Science, University of Tasmania, Hobart, Tasmania, Australia, <sup>2</sup>Courant Institute of Mathematical Sciences, New York University, New York, NY, USA, <sup>3</sup>Geophysical Fluid Dynamics Institute, and Earth, Ocean and Atmospheric Science, Florida State University, Tallahassee, FL, USA

**Abstract** Mixing by mesoscale eddies in the ocean plays a major role in setting the distribution of oceanic tracers, with important implications for physical and biochemical systems at local to global scales. Roach et al. (2016; <https://doi.org/10.1002/2015JC011440>) demonstrated that a two-particle analysis of Argo trajectories produces robust estimates of horizontal mixing in the Southern Ocean. Here we extend this analysis to produce global  $1^\circ \times 1^\circ$  maps of eddy diffusivity at the nominal Argo parking depth of 1,000 m. We also applied this methodology to estimate surface eddy diffusivities from Global Drifter Program (GDP) surface drifters. The global mean eddy diffusivity was  $543 \pm 155 \text{ m}^2/\text{s}$  at 1,000 m and  $2637 \pm 311 \text{ m}^2/\text{s}$  at the surface, with elevated diffusivities in regions of enhanced eddy kinetic energy, such as western boundary currents and along the Antarctic Circumpolar Current. The eddy kinetic energy at the equator is high at both the surface and depth, but the eddy diffusivity is only enhanced near the surface. At depth the eddy diffusivity is strongly suppressed due to the presence of mean flow. We used our observational estimates to test the validity of an eddy diffusivity parameterization that accounts for mixing suppression in the presence of zonal mean flows. Our results indicated that this parameterization generally agrees with the directly observed eddy diffusivities in the midlatitude and high-latitude oceans.

## 1. Introduction

The ocean plays an important role in the redistribution of heat, carbon (both natural and anthropogenic), and biogeochemical tracers. The evolution of these tracer fields on large spatial and time scales can be explained by mean passive tracer equations, averaged over time and spatial scales that are smaller than those of interest. This averaging introduces terms that represent the correlation of the velocity and tracer variability on scales shorter than the averaging scales—the eddy fluxes. These eddy fluxes are generally of first-order importance in setting the global tracer distributions and cannot be ignored (Gent & McWilliams, 1990; Gnanadesikan et al., 2013; Marshall & Speer, 2012; Speer et al., 2000). To form a closed system of equations, these eddy fluxes need to be parameterized as functions of the mean state. This is generally accomplished by using a down-gradient diffusion parameterization, where the eddy diffusivity is an externally imposed parameter. The role of this parameter is to crudely represent the influence of the dominant energy containing unresolved features, which in the ocean are the mesoscale eddies (Abernathey & Wortham, 2015) that are believed to be generated by baroclinic instability (Smith, 2007; Tulloch et al., 2011). A large body of theoretical work has been done to derive scalings for the eddy diffusivity itself based on the dynamics and mean flow (Ferrari & Nikurashin, 2010; Treguier et al., 1997; Visbeck et al., 1997). However, to validate the success of any of these theories, observational estimates of diffusivities are required.

Estimates of eddy diffusivity for the ocean have in the recent decade been obtained from both observations and high-resolution ocean-only models. The observational estimates have come from a diverse range of techniques, including altimetric measurements of sea surface height (SSH), where the SSH field is used to advect tracers and estimate the diffusivity (Abernathey & Marshall, 2013; Salée et al., 2011), and surface drifter, RAFOS float, and Argo float trajectories, where dispersion of Lagrangian particles are used to estimate the diffusivity (Chiswell, 2013; Davis, 1991; Katsumata & Yoshinari, 2010; Roach et al., 2016; Spall et al., 1993; Zhurbas & Oh, 2003). Other sources of observational eddy diffusivity estimates include Argo float hydrography, where a mixing length is estimated from the observed tracer variance and mean tracer gradients (Cole et al., 2015); ship-based hydrographic measurements, using inverse models (Faure & Speer, 2012) or tracer variance

**Table 1**

*Estimates of Ocean-Interior Horizontal Diffusivities on a Global Scale and in Four Specific Regions Compared to Our Results From Argo Floats and Cole et al. (2015) at 1,000 m*

Study	Diffusivity ( $\text{m}^2/\text{s}$ )	Error ( $\text{m}^2/\text{s}$ )	Study	Diffusivity ( $\text{m}^2/\text{s}$ )	Error ( $\text{m}^2/\text{s}$ )
<u>Global</u>			<u>Scotia Sea and DIMES</u>		
Groeskamp et al. (2017)	350	25	Naveira-Garabato et al. (2007)	1,840	440
Cole et al. (2015)	1,424		LaCasce et al. (2014)	800	200
(Cole et al. reduced by 2–3)	475–712		Tulloch et al. (2014)		
This study	543	155	(Second moment)	776	436
<u>Southern Ocean</u>			(Binned second moment)	664	520
Gille (2003)	422	130	Cole et al. (2015)	1,506	
Zika et al. (2009)	300	150	(Cole et al. reduced by 2–3)	502–753	
Cole et al. (2015)	2,551		This study	1,019	158
(Cole et al. reduced by 2–3)	850–1,276		<u>North Atlantic</u>		
This study	658	125	Zika et al. (2010)	0–200	
<u>South Pacific</u>			Armi and Stommel (1983)	500	
Faure and Speer (2012)			Spall et al. (1993)		
(Optimum inverse)	300	100	(Taylor's relationship)	330–380	
(Within CI of optimum)	200–800		(Float dispersion)	380–440	
Cole et al. (2015)	900		Cole et al. (2015)	712	
(Cole et al. reduced by 2–3)	300–450		(Cole et al. reduced by 2–3)	237–356	
This study	384	122	This study	356	142

*Note.* Grid cells with relative error over 0.75 or a mean number of pairs less than 10 have been excluded. Diffusivities quoted in this table for this study and Cole et al. (2015) are averages over the same geographical range as the first study listed for each region.

(Naveira Garabato et al., 2011); tracer release experiments, where an anthropogenic tracer is release and tracked (Ledwell et al., 1998; Tulloch et al., 2014); and natural tracer plumes, where tracer plume spreading from a natural source is related to diffusion (Naveira-Garabato et al., 2007). Estimates have also been obtained from high-resolution ocean models, which resolve the mesoscale and are run under realistic forcing and domains (Bates et al., 2014; Griesel et al., 2010).

Many of the observational estimates of eddy diffusivity are for specific regions (documented in Table 1), and global estimates that are available are generally limited to the ocean surface (SSH and surface drifter based). A few efforts have been made to obtain global observations of eddy diffusivity at depth. Cole et al. (2015) used the hydrographic data from Argo floats to obtain global estimates of eddy diffusivity extending from the surface to 2,000 m.

Here we use a Lagrangian framework and calculate cross-mean-flow relative diffusivities to obtain global estimates of eddy diffusivity at the surface and 1,000 m using surface drifter and Argo float trajectories. Surface drifters have been used previously to obtain global estimates of diffusivity at the surface (Zhurbas et al., 2014) using single-particle dispersion techniques. Argo float trajectories have not been used directly to estimate diffusivities in the past directly, as it was assumed that the profiling nature of these floats rendered them inadequate for this calculation. Chiswell (2013) instead estimated eddy diffusivities, at 1,000 m in the South Pacific and Indian Oceans, using a combination of Argo float displacements, Eulerian eddy statistics at the surface from SSH, and a relationship between Lagrangian and Eulerian timescales (Middleton, 1985). Roach et al. (2016) were able to show that Argo float trajectories could be directly used to get reasonable estimates of diffusivities in the Southern Ocean. Here we extend the analysis of Roach et al. (2016) to the global oceans. We then compared our global estimates to those from previous observational studies and tested theoretical ideas that have been proposed for predicting the observed eddy diffusivity based on the large-scale flow field (Ferrari & Nikurashin, 2010; Meredith et al., 2011).

## 2. Data

### 2.1. Argo Float Data

One of the major advances in observational oceanography in the last 20 years has been the development of the profiling float. The era of profiling floats started with the deployment of the Autonomous

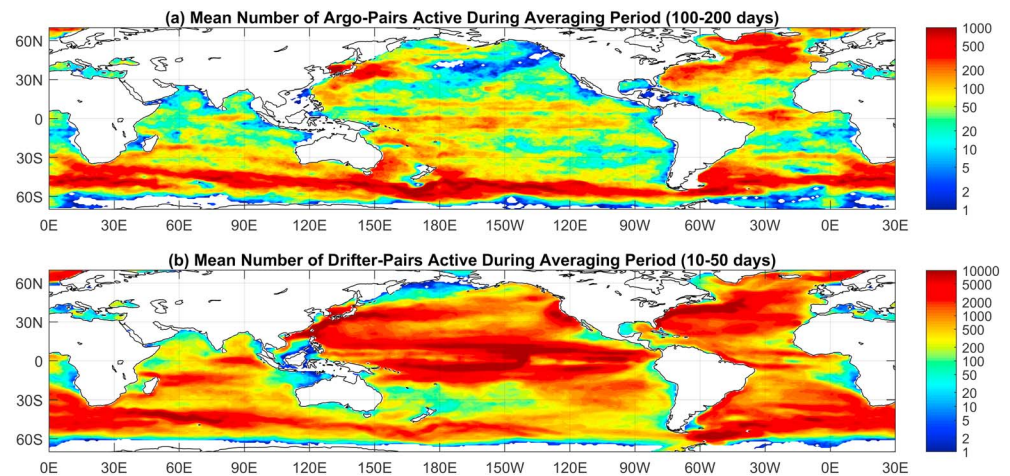


**Figure 1.** (a) Map of the number of Argo float-pairs active during the averaging period (100–200 days) used to compute  $K_h$  at 1,000 m. (b) Map of the number of drifter-pairs active during the averaging period (10–50 days) used to compute the near surface  $K_h$ .

Lagrangian Circulation Explorer (ALACE) floats (Davis, 1991), which measure temperature as they drift, during the World Ocean Circulation Experiment to track ocean currents. These were quickly superseded by the Profiling ALACE (PALACE) and Sounding Oceanographic Lagrangian Observer (SOLO) floats, which measure temperature and conductivity (salinity) profiles (Davis et al., 2001). The continued deployment, evolution, and data distribution are now carried out under the umbrella of the Argo program (Argo, 2000).

Argo floats are normally configured to operate on an approximately 10-day cycle. This cycle consists of multiple phases: a 3- to 4-hr descent to a parking depth (normally 1,000 m); 8–9 days of drift at parking depth; a profiling phase where the float descends to usually about 2,000 m, and then profiles to the surface over a 6-hr period; and finally, a data transmission phase lasting under an hour for iridium-equipped floats or about 6–12 hr for ARGOS-equipped floats.

The Argo data are processed and quality controlled to produce the user ready data sets. In this study, we use the August 2017 update of YoMaHa'07 data set (Lebedev et al., 2007). This data set contains approximately 135,000 surface location fixes from 9,898 floats deployed between 1998 and early 2017. The mean cycle time over all data was 9.2 days, with 78% of cycles having a parking time of between 11 and 12 days. The mean programmed parking depth was 1,038 m. The mean float lifespan, including recently deployed floats, was 1,294 days or 1,513 days if floats deployed after August 2014 were excluded. The number float-pairs present during the averaging period (100–200 days; see section 3.2) are shown in Figure 1a.

## 2.2. Drifter Data

The Global Drifter Program (GDP) has been responsible for deployment and maintenance of a surface drifter array to measure the surface currents. We use the AOML compilation (Lumpkin et al., 2013) of the data that extends up to September 2016. This data set predominantly consists of SVP type drifters with a holey-sock-type drogue centered at 15 m depth. For our analysis we only used the drifter trajectories for which the drifter's drogue was still attached, in order to estimate mixing within the upper ocean while reducing contamination from windage. We used trajectories from a total of 17,201 drifters, over 70% of which were deployed after 2000.

Drifters had a mean (median) lifespan, here taken as the shorter of the time until the drogue was lost or the drifter stopped transmitting, of about 190 days (120 days). However, we found that drifter lifespan varied significantly over the course of the GDP, peaking at 368 days for drifters released in 1995 and showing a minimum of 97 days in 2006. The mean number float-pairs present during the averaging period (10–50 days; see section 3.2) are shown in Figure 1b.

### 3. Methods

#### 3.1. Estimating Diffusivity Using A Two-Particle Principal Component Approach

Eddy diffusivity quantifies the rate of spreading of a cloud of tracer or particles under the action of turbulent processes. Taylor (1921) showed that under the assumption of a smooth mean tracer field and only local influences of the mean tracer field on the tracer fluxes, the effect of turbulent velocity fields on tracer spreading could be parameterized as a down-gradient diffusion. The simplicity and ease of implementation associated with this parameterization have led to its wide spread use in representing unresolved turbulent processes in models (Fox-Kemper et al., 2013).

Lagrangian trajectories of particles can be used to estimate the eddy diffusivity in the ocean (Davis, 1991; LaCasce, 2008). The general idea is to estimate the rate of dispersion following the center of mass of a collection of particles:

$$K(t) = \frac{1}{2} \frac{d}{dt} \overline{X(t)^2} \quad (1)$$

where  $K$  is the diffusivity and  $X$  is particle distance relative to the center of mass. This estimate of diffusivity is referred to as a *single-particle* measure of diffusivity. This definition can be expressed in other equivalent forms, such as a time integral of the velocity autocorrelation, or a correlation of velocity and displacement. In a long-time limit, for an isotropic and homogeneous turbulent field, all these definitions will give the same result (LaCasce et al., 2014). For an anisotropic field the eddy diffusivity can be expressed as a tensor, to account of the varying dispersion rates in different directions and rotation of the coordinate frame relative to the direction of the greater eddy diffusivity.

In practice, the flow field is rarely homogeneous, data sampling does not extend to infinite time, and defining an appropriate background flow field is challenging (Balwada et al., 2016; LaCasce et al., 2014; Rypina et al., 2012). In our diffusivity calculation method described below (see also Roach et al., 2016) we aim to mitigate the errors and biases associated with these issues.

We use relative dispersion instead of single-particle dispersion in practice because an explicit definition of the mean velocity field or center of mass of particles is not required when using relative dispersion, and this helps to reduce the errors associated with defining the mean flow (LaCasce, 2008). At short times, the relative dispersion is able to quantify the role of the spatially correlated velocity field in stirring the particles, which is not possible with the single-particle dispersion. However, at long times, the regimes that we are interested in, the single-particle and relative dispersions, provide the same information: relative diffusivity being greater than the single-particle diffusivity by a factor of 2. For each collection of trajectories (details of this selection are presented in the next section), at each time step, we construct a relative dispersion tensor,

$$\begin{bmatrix} d_x^2 & |d_x| \cdot |d_y| \\ |d_x| \cdot |d_y| & d_y^2 \end{bmatrix},$$

where  $d_x$  and  $d_y$  denote the zonal and meridional components of particle separation for each pair and  $\langle \rangle$  indicates averaging over all pairs.

We further calculate the eigenvalues of the relative dispersion matrix, denoted as  $\lambda$ . This helps to orient relative dispersion tensor along the dominant direction of dispersion growth. This direction is generally the direction of the mean flow, as the shear of the mean flow greatly enhances the dispersion associated with the background isotropic turbulent field in the along mean flow direction (Bolster et al., 2011; Young & Jones, 1991; Zhurbas et al., 2014). We calculate the relative diffusivity as

$$K_{\text{rel}}(t) = \frac{\lambda(t) - \lambda(0)}{2t}, \quad (2)$$

where  $\lambda(0)$  is the eigenvalue at initial time, representing the initial size of the particle patch. The long-time diffusivity, when particle pair trajectories have decorrelated and the diffusivity asymptotes to a constant, is the measure of diffusivity that represents the influence of the turbulent velocity field on the mean tracer

equation. In the presence of a shear flow, only the smaller of the two diffusivities associated with the two eigenvalues approaches a constant, which is twice the single-particle diffusivity (LaCasce, 2008), hence:

$$K(\infty) = \min\left(\frac{K_{\text{rel}}(\infty)}{2}\right). \quad (3)$$

The greater value corresponds to shear diffusion, which grows without bounds.

In practice, the  $K(\infty)$  (hereafter designated  $K_h$ ) needs to be evaluated at a fixed interval at large time because over time the floats disperse from the region of interest, or the vicinity of the grid point, and instrument failure leads to finite time series of float trajectories. This fixed large time needs to be significantly greater than the Lagrangian integral time, because the value of the eddy diffusivity oscillates in time and can take much longer to asymptote to a fixed value (Klocker et al., 2012; LaCasce et al., 2014; Zhurbas et al., 2014). We describe our choice of this evaluation time period in the next section.

### 3.2. Implementation

The calculation of eddy diffusivity using the algorithm described above requires a number of practical choices to be made, when applying to finite time data sets in the ocean that sample an anisotropic and inhomogeneous turbulent velocity field. These choices and the rationale behind them are described in this section.

We first grid the ocean into  $1^\circ$  by  $1^\circ$  bins. At each grid point, the center of the bin, we identified all floats that passed within a circle of radius 200 km. Each identified float trajectory was then subsampled to isolate the period between when the float first entered the 200 km radius, up to when the distance between the float and grid-point exceeded 1,000 km. The first data point in this selected trajectory was marked as day 0 corresponding to the grid point. As the identified and isolated float trajectories span a region greater than the size of the grid, this choice of trajectory sampling is comparable to a nonuniform weighted running mean. The region of influence that contributes to the calculation at the grid point is in an ellipse that is approximately 1,200 km by 400 km in size and extends downstream of the grid point. The weights in the averaging decrease away from the grid point, as most number of trajectories will be concentrated near the grid point. We discuss the characteristic size of the region that contributes to the calculation of eddy diffusivity at each grid point in the results. This sampling choice helps in obtaining a smooth result, while also accounting for the kinematic fact that during the stirring process, the fluid is advected into the region near the grid point, stirred by the local diffusivity, and then advected out by the mean flow.

Next we designate the selected trajectories into pairs to calculate the relative dispersion matrix. This was done by designating pairs from trajectories that had their starting location, when they enter the region within 200 km of the grid point, within 100 km of each other. The choice of 100 km is approximately the size of the ocean mesoscale eddies and approximates the length scales over which the fluid velocities are spatially uncorrelated. Also, we decided to consider a pair from two trajectories that might have passed through the region at different times, extending up to the oldest and most recent floats passing through a given bin. Usually, in relative dispersion studies, only the simultaneous trajectories with small initial separations are considered, as the primary interest is in the influence of the correlated motion on dispersion (LaCasce & Bower, 2000; Ollitrault et al., 2005). However, we are interested in the long-term uncorrelated behavior, so our choice of trajectories for pairs that are uncorrelated initially, due to a wide separation in time or space of the initial point, is justified. Here we are making the inherent assumption that the eddy diffusivity is a constant in time, and low-frequency temporal variability does not significantly influence the mean or eddy field. We cannot presently relax this choice because of the limited density and coverage of the Argo float data.

Time series of zonal, meridional, and absolute particle separation were then computed at 5-day (drifter) or 10-day (Argo) intervals for each particle pair. These separation time series make up the relative dispersion matrix. The eigenvalues of the relative dispersion matrix were calculated, and the smaller eigenvalue was used to estimate the eddy diffusivity as a function of time (equation (2)).

Prior estimates of isopycnal mixing using Argo trajectories (Chiswell, 2013; Katsumata & Yoshinari, 2010) estimated diffusivities using statistics over the course of one Argo cycle (approximately 10 days), which is close to the Lagrangian integral time scale. However, studies using numerical particles and RAFOS float (Balwada



et al., 2016; LaCasce et al., 2014; Spall et al., 1993) indicate that single and relative diffusivity time series generally show a peak in time before settling to a significantly lower asymptotic value. The time when this value is realized is approximately 70 to 100 days at depths of about 1,000 m (LaCasce et al., 2014), and 10–20 days near the surface (Zhurbas et al., 2014), and varies regionally. Figure 1 shows maps of the number of float (Figure 1a) and drifter (Figure 1b) pairs that were available for this calculation. Taking this fact about the nature of the diffusivity, or velocity autocorrelations, into account, we opt to take the asymptotic diffusivity as the mean between 100 and 200 days for Argo floats, and 10–50 days for the surface drifters. Maps showing the diffusivity as a function of time, and a qualitative validation for this choice, are presented in Figures S3 and S4. This asymptotic eddy diffusivity is the central calculation of this study.

We assessed the uncertainty in this diffusivity estimate using a bootstrap process. A float was randomly selected, all pairs including that float were dropped, the remaining data were resampled allowing for repetition, and another estimate of diffusivity produced. This process was repeated 100 times with randomly selected floats, and then the uncertainty in the diffusivity was taken as the resulting two standard deviation range.

Apart from the statistical errors, which are quantified using the bootstrapping method, there are errors associated with the profiling of the Argo floats. While none of the Lagrangian instruments that have been developed so far follow the water parcels precisely, the Argo floats are particularly questionable due to their vertical profiling cycle. However, if the time spent away from the parking depth is short relative to the time spent at the parking depth, as show in section 2 of the supporting information, the error introduced by the vertical cycling (Figure 2e) is comparable to the statistical error (Figure 2b). The two errors have different spatial patterns, as one quantifies the uncertainty due to sampling issues and the statistical nature of the quantity being sampled, while the other due to the differences between the velocity field at the surface and at depth.

To compare our results against the mean flow or eddy energy, we produced gridded fields of interior and near-surface mean flow ( $U_M$ ) by averaging YoMaHa'07 Argo velocities and drifter velocities in regular  $1^\circ \times 1^\circ$  bins. Eddy kinetic energy (EKE) was obtained by taking the difference between the observed float or drifter velocities and the corresponding interpolated  $U_M$ .

### 3.3. Mixing Suppression Theory

Parameterizations of eddy diffusivity attempt to relate the magnitude of the eddy diffusivity to some large-scale variables, such as the slope of the isopycnals (Visbeck et al., 1997), background potential vorticity gradients (Srinivasan & Young, 2014), and large-scale mean flow (Ferrari & Nikurashin, 2010; Meredith et al., 2011). In this section we specifically focus on testing the prediction that the eddy mixing length scale is suppressed in the presence of a background mean flow (Ferrari & Nikurashin, 2010; Meredith et al., 2011).

Ferrari and Nikurashin (2010) showed that in a quasi-geostrophic framework, a broad, time-mean jet in the presence of propagating eddies suppresses the lateral diffusivity that would otherwise result only due to the propagating eddies. Rypina et al. (2007) suggested that the suppression should be present even if there is no scale separation between the mean flow and eddies. Ferrari and Nikurashin (2010) derived the following expression for the effective diffusivity ( $K_{\text{eff}}$ ), resulting from a combination of a mean flow ( $U_M$ ) and unsuppressed diffusivity ( $K_0$ ),

$$K_{\text{eff}} = \frac{K_0}{1 + \gamma^{-2} k^2 (U_M - c)^2}. \quad (4)$$

where  $K_0$  is defined using simple mixing length arguments as

$$K_0 = \frac{k^2}{(k^2 + l^2)} \frac{\text{EKE}}{\gamma}; \quad (5)$$

EKE denotes the EKE,  $\gamma$  denotes the linear eddy damping rate (representing nonlinear damping through eddy-eddy interactions),  $c$  denote the eddy phase speed, and  $(k, l)$  is the horizontal wave vector of the eddy field.

Apart from the eddy damping rate, the parameters required to estimate the effective diffusivity can be obtained directly from existing data sets. Following previous studies (Ferrari & Nikurashin, 2010; Meredith

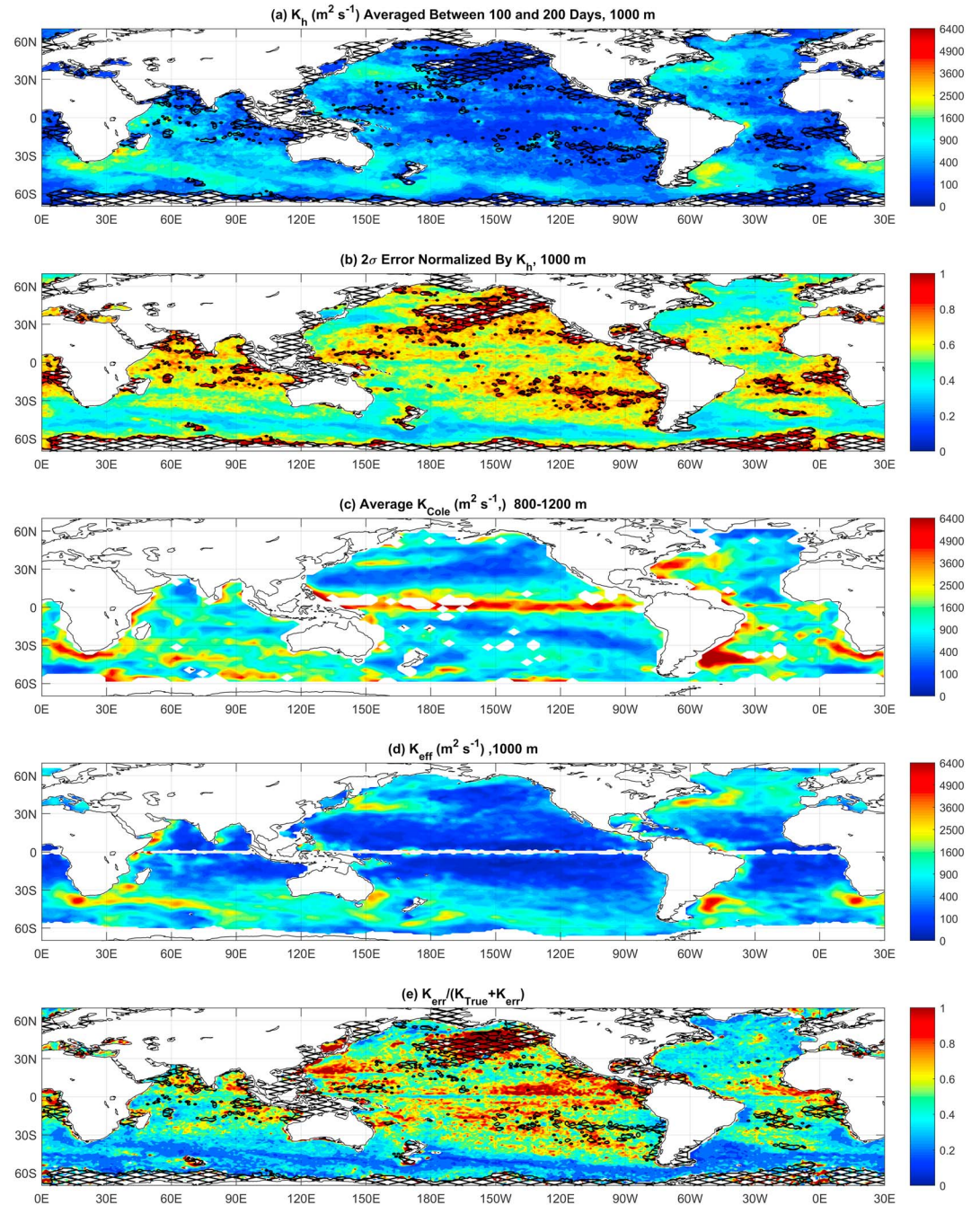


**Figure 2.** (a) Global map of cross-stream diffusivity ( $K_h$ ) at nominal 1,000 m averaged between 100 and 200 days post-release. (b)  $2\sigma$  error normalized by cross-stream diffusivity. (c) Estimates of diffusivity from Cole et al. (2015) averaged between 800 and 1,200 m. (d) Diffusivity including mean-flow suppression ( $K_{\text{eff}}$ ) estimated using equation (7). (e) Error induced by profiling ( $K_{\text{err}}$ ) normalized by equivalent observed error ( $K_{\text{true}} + K_{\text{err}}$ ). Hatched regions in (a), (b) and (e) indicate regions with  $2\sigma$  error  $>75\%$  of  $K_h$  or with a mean number of float-pairs active during the averaging period (100–200 days) less than 10.

et al., 2011), we use an empirical relationship between eddy damping rate, wave number, and EKE and define the damping rate as an eddy turn over time,

$$\gamma^{-2}k^2 \approx \frac{4}{\text{EKE}}. \quad (6)$$

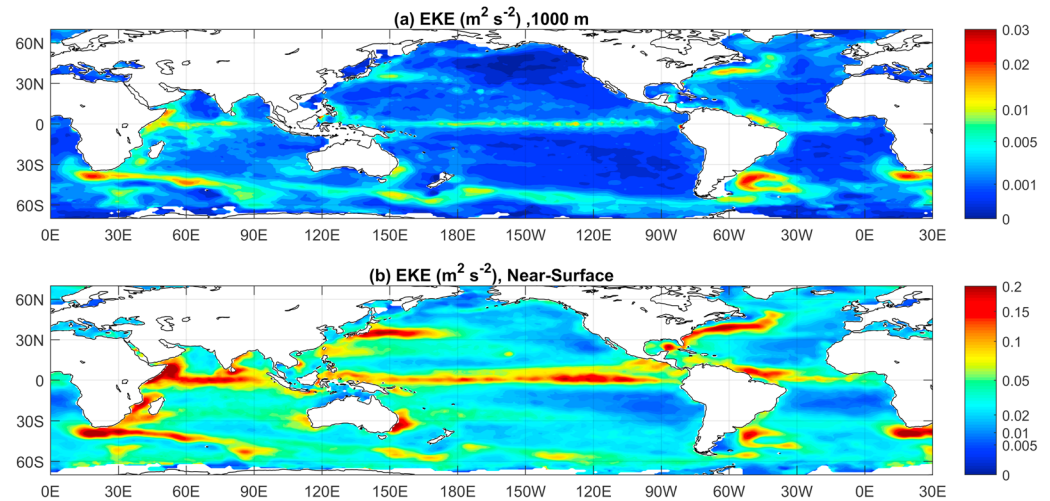


**Figure 3.** Maps of eddy kinetic energy ( $\text{m}^2/\text{s}^2$ ) (a) at 1,000 m and (b) in the near-surface layer.

Additionally, we assume that the eddy field is isotropic and  $k = l = \frac{2\pi}{L_{\text{eddy}}}$ , where  $L_{\text{eddy}}$  is the twice the eddy radius. Under these assumptions the expression for effective diffusivity becomes

$$K_{\text{eff}} = \frac{2\sqrt{\text{EKE}}}{k \left( 1 + 4 \frac{(U_M - c)^2}{\text{EKE}} \right)} \quad (7)$$

The above expression can be evaluated using observations. In addition to the mean flow and EKE estimated from the Yomaha'07 data set, the eddy radius from Chelton et al. (2011) (Version 4, 2017 one-day resolution update) and phase speed (Fu, 2009) estimate from SSH fields were interpolated to the  $1^\circ$  grid of this study. These variables were then interpolated onto the Argo float and surface drifters, so that equations (5) and (7) could be evaluated following each float/drifter. The  $K_{\text{eff}}$  and  $K_0$  evaluated along each trajectory were averaged onto each grid point using only the segments of the trajectories that had contributed to the diffusivity estimate for that grid point. This procedure is necessary so that  $K_{\text{eff}}$  and  $K_0$  were influenced by the same range of dynamics as  $K_h$ .

## 4. Results

### 4.1. Horizontal Mixing at 1,000 m From Argo Floats

Maps of horizontal eddy diffusivity,  $K_h$ , at 1,000 m, averaged between 100 and 200 days, and the corresponding  $2\sigma$  confidence intervals, normalized by the estimate of the eddy diffusivity, based on bootstrapping are shown in panels a and b (respectively) of Figure 2. Hatching in Figures 2a, 2b, and 2e indicates regions where either the  $2\sigma$  confidence interval is greater than 75% of  $K_h$  or the number of float-pairs present during averaging was less than 10. The eddy diffusivity shows a strong regional variability that is associated with the patterns of EKE (Figure 3a); higher EKE is collocated with regions of strong mean flows. Larger diffusivity is observed in the energetic extensions of the western boundary currents and the Antarctic Circumpolar Current, and smaller diffusivity in the less energetic eastern sides of the gyres.

The confidence intervals indicate small, 10–30%, uncertainty in areas of high data density, and slightly greater, 30–50%, uncertainty in regions of lower data density. Occasional spikes of more than 100% uncertainty are present for grid cells in which very few float-pairs remained within 1,000 km during the averaging period. The maps of uncertainty show visual anticorrelation with maps of eddy diffusivity. This is because greater diffusivity is generally associated with regions of strong mean flows, which leads to increased sampling as more floats are advected through these regions.

The eddy diffusivity estimate at each grid point is an average over a region sampled by the floats that pass in the vicinity of the grid point; the exact estimation strategy was explained in section 3. However, as the



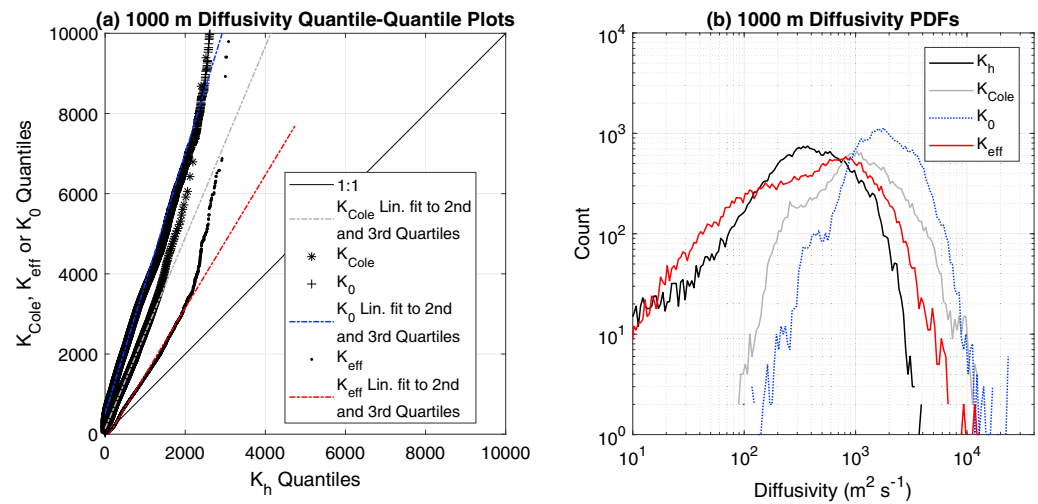


**Figure 4.** (a) QQ plot comparing our estimated 1,000 m diffusivity to Cole's estimates ( $K_{Cole}$ , grey line, asterisk), mixing suppression theory ( $K_{eff}$ , red line, dots), and theory without suppression ( $K_0$ , blue line, crosses); individual quantiles are shown as symbols, while linear fits to quantiles between the second and third quartiles are shown as lines. (b) Histograms of 1,000 m diffusivities from our estimates ( $K_h$ , black), Cole's estimates ( $K_{Cole}$ , grey), mixing suppression theory ( $K_{eff}$ , red), and theory without suppression ( $K_0$ , blue).

kinematics of each region are different, the distribution of the floats in the vicinity of the grid point, that is, the sampling weight at the time when the eddy diffusivity is estimated, is different. We plotted the characteristic scale of the sampling density, root-mean-square of the float pair separation, as a global time series (Figure S2a) and as a map (Figure S2c) during the averaging period in the supporting information. Away from the equator, the characteristic scale is 300–600 km; by way of comparison, the global mean eddy diameter from Chelton et al. (2011) is about 170 km, so our scales are about 2–4 times the size of a typical eddy. This characteristic scale gives a coarse upper-bound estimate of the length scales that the eddy diffusivity estimates are associated. It is an upper bound because the diffusivity theoretically asymptotes to a constant at length scales greater than the size of the largest eddies. This characteristic length scale will also be inflated in regions of strong zonal shear, but our diffusivity estimate would be a measure of processes that acted in the cross-stream direction on a relatively smaller scale.

We also tested the influence of the time period, average over 100–200 days, that was chosen to represent the asymptotic diffusivity estimate. Examination of maps of  $K_h(t)$  at different times over the integration period (Figure S3) indicates that the structure of isopycnal mixing and amplitudes of mixing in weak mixing regions display little or no sensitivity to integration time after about 50–100 days. Mixing amplitudes in regions of strong mixing tend to be reduced slightly at longer integration times, as the spreading of floats over time includes contributions from adjacent regions of weaker mixing.

We compared our observed diffusivities at 1,000 m to the  $3^\circ$  resolution fields produced by Cole et al. (2018) using the methodology described in Cole et al. (2015), averaged between depths of 800–1,200 m. Cole et al. (2015) estimated the diffusivity by calculating a length scale from Argo hydrography, defined as the salinity variance divided by the mean salinity gradient along isopycnals, using the estimate of EKE from the  $1/4^\circ$  ECCO2 model state estimate, and a mixing efficiency of 0.16. This diffusivity estimate is representative of a diffusivity that acts across the mean salinity contours on isopycnals.

Our diffusivity estimates agree in structure with Cole et al. (2015) at mid-to high latitudes, with our estimates being slightly smaller in magnitude (compare Figures 2a and 2c). Cole et al. (2015) displayed a region of high diffusivity along the equator in the Pacific Ocean, which we did not observe in our results. This is likely an effect of their methodology, which can produce very large estimates when the tracer gradients are weak, as is the case at 1,000 m in the equatorial region. Figure 4a shows quantile-quantile (QQ) plots of our data versus Cole et al. (2015) estimates interpolated to our  $1^\circ \times 1^\circ$  grid. QQ plots (Wilk & Gnanadesikan, 1968) were constructed by computing the cumulative distribution functions for each data set, dividing the cumulative distribution functions into regularly spaced quantiles (probability bins) and then identifying the parameter-

values which correspond to each quantile. The QQ plot shows a relatively linear relationship between the quantiles of our estimates and Cole's, implying that the two have a similar type of distribution. Both histograms (Figure 4b) and QQ plots demonstrated suggest that Cole's isopycnal diffusivities are typically 2.5 times larger than our results.

This difference in magnitude can be attributed to a number of reasons. It could be a result of differences in methodology; Klocker and Abernathey (2014) have noted (their appendix B) that the method of defining the length scale based on tracer variance produces diffusivities that are generally greater by a factor of 2–3 than those obtained by more direct estimates, such as those based on tracer contour stretching or Lagrangian estimates. It is possible that the EKE field produced in ECCO2 is different from those observed in the oceans. There may also be some contribution from differences in spatial scales between this study and Cole et al. (2015). It is also possible that the differences occur because our results are indicative of diffusivities that are across mean streamlines, while Cole et al. (2015) is indicative of diffusivities that are across mean salinity contours. However, a comparison (not shown) of 1,000 m salinity contours and geostrophic stream function (Gray & Riser, 2014) suggests that salinity and mean geostrophic streamlines are generally aligned with each other, except at very low latitudes, implying that our two diffusivity estimates should be comparable.

We also compared our results with other prior observational estimates of horizontal/isopycnal diffusivity within the ocean interior for various regions (Table 1). These studies used a variety of methodologies, including inverse modeling (Faure & Speer, 2012; Groeskamp et al., 2017; Zika et al., 2009, 2010), RAFOS float trajectories (LaCasce et al., 2014; Spall et al., 1993), and tracer measurements (Armi & Stommel, 1983; Gille, 2003; Naveira-Garabato et al., 2007; Tulloch et al., 2014). Also, included in Table 1 are 1,000 m regionally averaged diffusivities from both the gridded estimates of horizontal mixing described in this study and in Cole et al. (2015).

Our global analysis agreed with regional studies where methodologies were compatible. Results matched well with Groeskamp et al. (2017), Gille (2003), Faure and Speer (2012), Zika et al. (2010), Spall et al. (1993), Tulloch et al. (2014), and LaCasce et al. (2014) within  $2\sigma$  confidence intervals. While our results were larger and did not agree with Zika et al. (2009) within the chosen error bars, the difference can be explained by our choice of averaging over a wider meridional range. While agreeing closely with the DIMES experiments in the Drake Passage and Scotia Sea, our results were smaller than those of Naveira-Garabato et al. (2007), who estimated isopycnal mixing between the  $\gamma_N$  27.73–28.0 kg/m<sup>3</sup> surfaces in the same region. The depth of this water-mass varied between 1300–2,000 m in the north of the region and 300–500 m on the Antarctic margins, implying that Naveira-Garabato et al. (2007) sampled mixing within both the ocean interior and near-surface layers, likely explaining the difference. With reduction by a factor of 2 to 3, Cole et al.'s (2015) diffusivities were broadly consistent with our estimates and prior studies in the global mean and regional cases.

#### 4.2. Near-Surface Lateral Mixing From GDP Drifters

Maps of horizontal diffusivity at the surface, averaged between 10 and 50 days, and the corresponding  $2\sigma$  confidence intervals, normalized by the estimate of the eddy diffusivity, based on bootstrapping are shown in Figures 5a and 5b, respectively. This diffusivity estimate is a result of the geostrophic circulation associated with the oceanic mesoscale eddy field, and also the ageostrophic velocities associated with the Ekman flows and submesoscale, larger Rossby number flows. As with ocean interior mixing, discussed above, areas of enhanced mixing are frequently associated with areas of elevated surface EKE (Figure 3b). The near-surface mixing displays a band of exceptionally strong mixing (8,000–15,000 m<sup>2</sup>/s) in proximity to the equator in all major ocean basins, which is not present at 1,000 m. Strong near-equatorial horizontal mixing has been seen in other observational studies using surface drifters (Zhurbas et al., 2014), but not in mixing estimates from SSH-derived velocity fields that only account for the geostrophic component of the ocean velocities (Abernathey & Marshall, 2013). Equatorial regions are usually associated with divergent winds (Hastenrath & Lamb, 1978; Zheng et al., 1997), suggesting that the enhanced dispersion of surface drifters might be produced by wind-driven flow rather than by mesoscale eddies.

The uncertainty estimates are generally smaller than 30%, and much smaller relative to the uncertainty in diffusivity estimates at 1,000 m from Argo floats. The greater confidence is a result of a larger number of surface drifters relative to Argo floats. Similar to the uncertainty from Argo floats, the uncertainty maps from surface drifters are qualitatively anticorrelated with the diffusivity estimates.

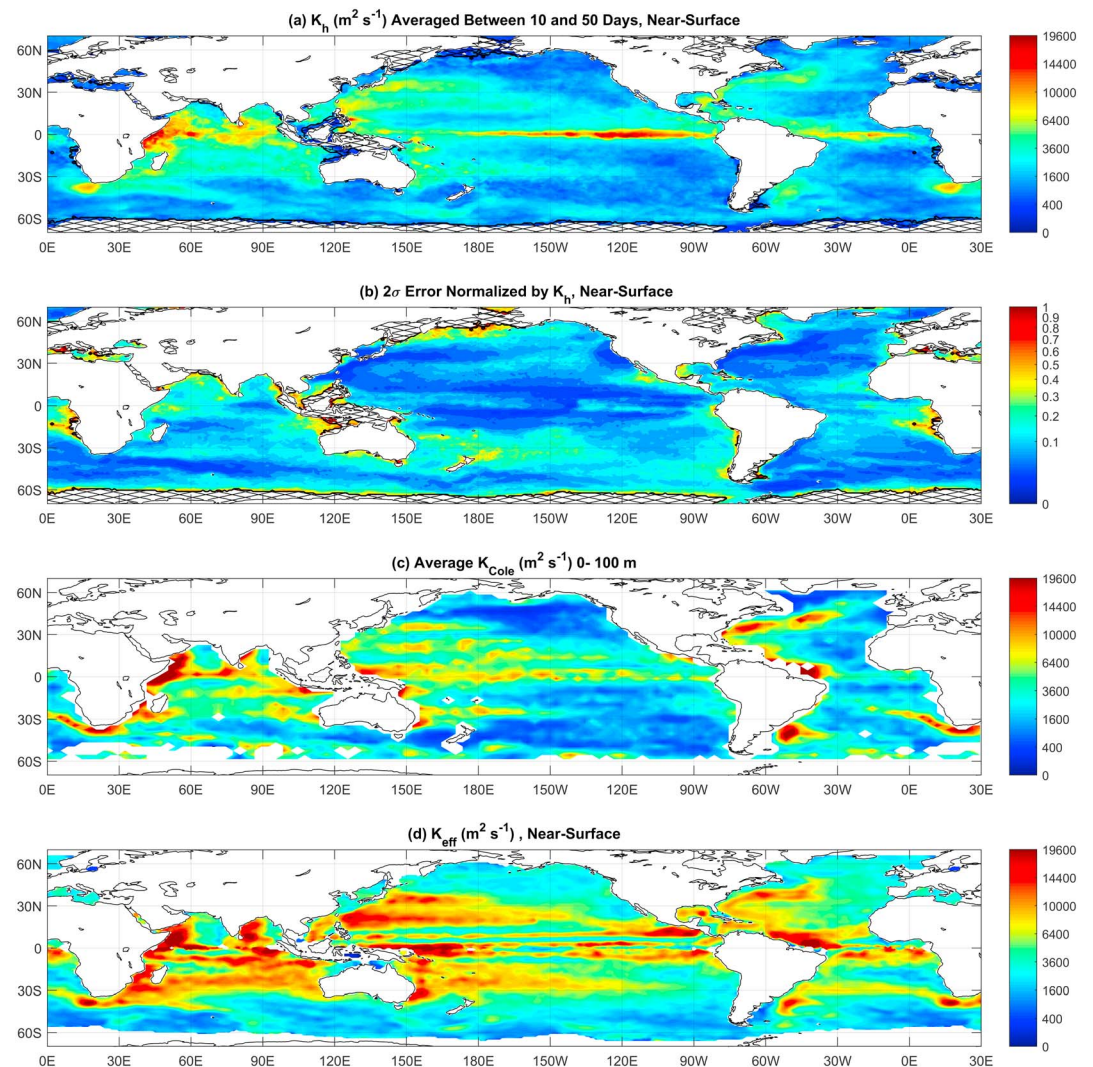


**Figure 5.** (a) Global map of near-surface cross-stream diffusivity ( $K_h$ ) averaged between 10 and 50 days postrelease. (b)  $2\sigma$  error normalized by cross-stream diffusivity. (c) Estimates of diffusivity from Cole et al. (2015) averaged over the upper 100 m. (d) Horizontal diffusivity including mean-flow suppression estimated using equation (7). Hatched regions in (a) and (b) indicate regions with  $2\sigma$  error  $>75\%$  of  $K_h$  or with a mean number of drifters active during the averaging period (10–50 days) less than 10.

To confirm our choice of integration and averaging periods, we plotted maps of drifter  $K_h(t)$  between 10 and 80 days (Figure S4). Mixing structure and magnitude were found to be coherent and stable out until about 50 days, indicating that the eddy diffusivity approached its asymptotic value. Thereafter, mixing magnitude rapidly fell, and previously robust structures became patchy, due to a combination of short drifter lifespans and relatively rapid dispersion spreading floats beyond our upper sampling radius (1,000 km). The global characteristic scale, root-mean-square of drifter-separation (Figures S2a and S2b), during the 10- to 50-day averaging period was between 350 and 700 km, with large particle separations (600–900 km) seen near the equator and in areas of high EKE, and smaller values (200–500 km) seen over the majority of the ocean.

The structure of our horizontal diffusivity estimates generally agree (Figures 5a and 5c) over all ocean basins with those from Cole et al. (2015). Slopes of the QQ plot (Figure 6a) and comparison of histograms (Figure 6b) from our estimates of mixing and Cole et al. (2015) show that the diffusivity from Cole et al. (2015) is greater by a factor of approximately 2, similar to the difference seen at 1,000 m. Diffusivity from Cole et al. (2015) skew large relative to our observations in the Gulf Stream, Brazil-Falklands Confluence, Agulhas retroflection, and Somali current, while (Cole et al., 2015) underestimates mixing, relative to our estimates, in proximity to the equator in the Pacific.

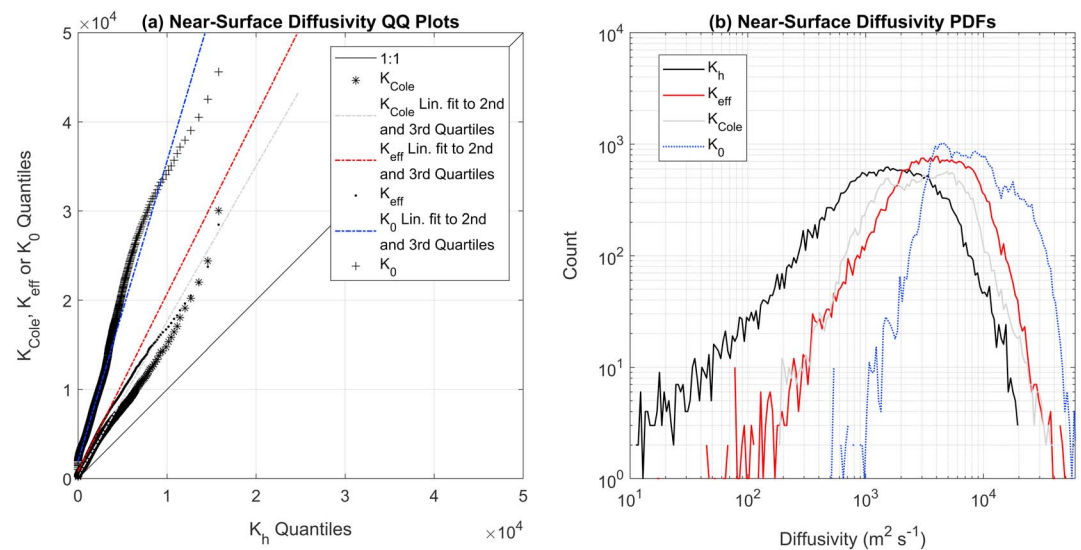


**Figure 6.** (a) QQ plot comparing our estimated near-surface diffusivity to Cole's estimates ( $K_{\text{Cole}}$ , grey line, asterisk), mixing suppression theory ( $K_{\text{eff}}$ , red line, dots), and theory without suppression ( $K_0$ , blue line, crosses); individual quantiles are shown as symbols, while linear fits to quantiles between the second and third quartiles are shown as lines. (b) Histograms of near-surface diffusivities from our estimates ( $K_h$ , black), Cole's estimates ( $K_{\text{Cole}}$ , grey), mixing suppression theory ( $K_{\text{eff}}$ , red), and theory without suppression ( $K_0$ , blue).

We also compared our data to maps produced by Zhurbas et al. (2014), from surface drifter data using single-particle statistics, and Abernathey and Marshall (2013), from SSH-derived velocity fields. The results of this study were generally consistent in both structure and magnitude with the diffusivity estimated by Abernathey and Marshall (2013), excluding the near-equatorial bands discussed above. The structure of our  $K_h$  fields agreed with maps of maximum lateral and asymptotic diffusivity obtained by Zhurbas et al. (2014), while the magnitude of our estimates was more consistent with their asymptotic diffusivities.

### 4.3. Comparison to Diffusivity Parameterizations: Mixing Suppression

Visual comparison of the maps of eddy diffusivity estimated from observations, Argo floats, and surface drifters, and by evaluating equation (7) (Figures 2d and 5d) using observations demonstrated good agreement in spatial structure, in the midlatitude and high latitude away from the equator. The agreement in magnitude was reasonable for the Argo floats, but poor for the surface drifters. The inconsistency in mixing structure at low latitude between our observations and theory is likely associated with low-latitude ocean equatorial dynamics being dominated by Kelvin waves, which might not be modeled appropriately by the stochastic model that was considered in Ferrari and Nikurashin (2010). Unsuppressed diffusivity ( $K_0$ ) (Figures 7a and 7b) displayed some agreement in structure with the observed diffusivity, as it is enhanced in region of higher EKE, but drastically overestimated the magnitude over much of the ocean.

Plots of diffusivity as a function of EKE (Figure 8) further confirm the visual comparison, for both the near surface and at 1,000 m; our observed diffusivities were consistent with suppressed diffusivities ( $K_{\text{eff}}$ ; equation (7)), and not consistent with unsuppressed diffusivities ( $K_0$ ; equation (5)). This is also emphasized by examination of QQ plots (Figures 4a and 6a) and probability density functions (Figures 4b and 6b). QQ plots indicated a predominantly linear relationship between observed eddy diffusivities and both suppressed and unsuppressed theoretical diffusivities, with deviations from linear behavior associated with the largest 5% of the data. The slopes of QQ plots also emphasized a magnitude difference, with unsuppressed diffusivities ( $K_0$ ) typically being 3 times larger than our ocean interior observations and 3.5 times larger than our near-surface observations. Suppressed diffusivities ( $K_{\text{eff}}$ ) tended to be approximately 1.5 times larger than our ocean interior observations and 2 times larger than our near-surface observations.

The differences between our observed diffusivities and the expression for suppressed diffusivity could result from a number of reasons. The eddy radius used in this could be as overestimate of the dominant eddy



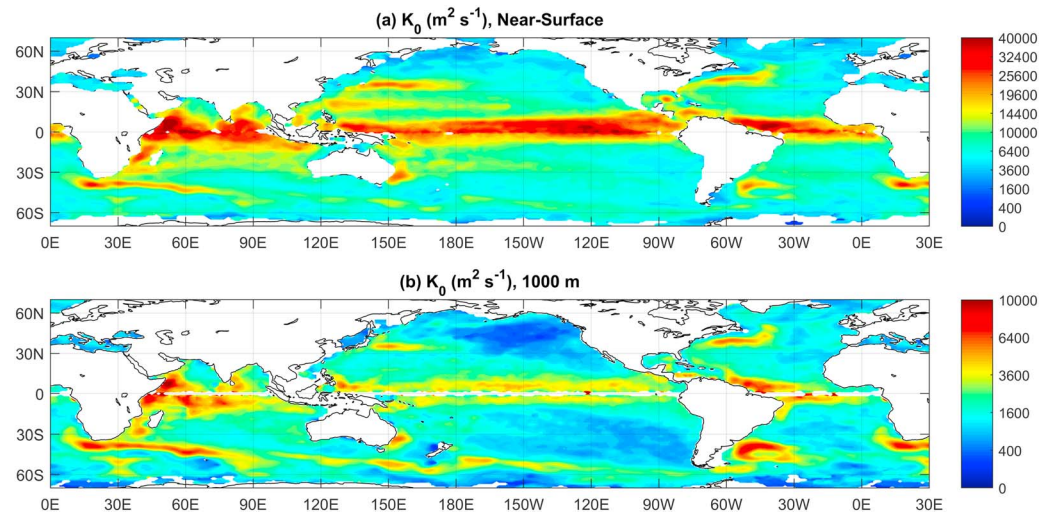


**Figure 7.** Maps of unsuppressed ( $K_0$ ) eddy diffusivity computed from equation (5) (a) in the near-surface layer and (b) at 1,000 m.

length scale due to the limited spatial resolution ( $1/4^\circ$ ) of the SSH fields that are used to derive it. The presence of a significant anisotropy in the turbulent field can render the assumptions used to approximate  $K_{\text{eff}}$  invalid. A better agreement at depth, than near the surface, could be a result of ageostrophic flows, winds, and high Rossby number flows, influencing the observed eddy diffusivity near the surface.

We conclude that our observations are broadly consistent with the scaling theory (Ferrari & Nikurashin, 2010; Meredith et al., 2011) incorporating suppression of mixing by mean flow, and some adjustments to expression might be required for better quantitative agreement.

## 5. Discussion and Conclusion

In this study we present global observational estimates of Lagrangian eddy diffusivity at the surface and 1,000 m from GDP surface drifters and Argo floats on a  $1^\circ$  grid. The eddy diffusivity at the Argo parking depth, 1,000 m, has a global mean of  $543 \pm 155 \text{ m}^2/\text{s}$  and range between the 10th and 90th percentiles of 100–1,000  $\text{m}^2/\text{s}$ , and at the surface has a global mean of  $2637 \pm 311 \text{ m}^2/\text{s}$  and 10th to 90th percentile range of

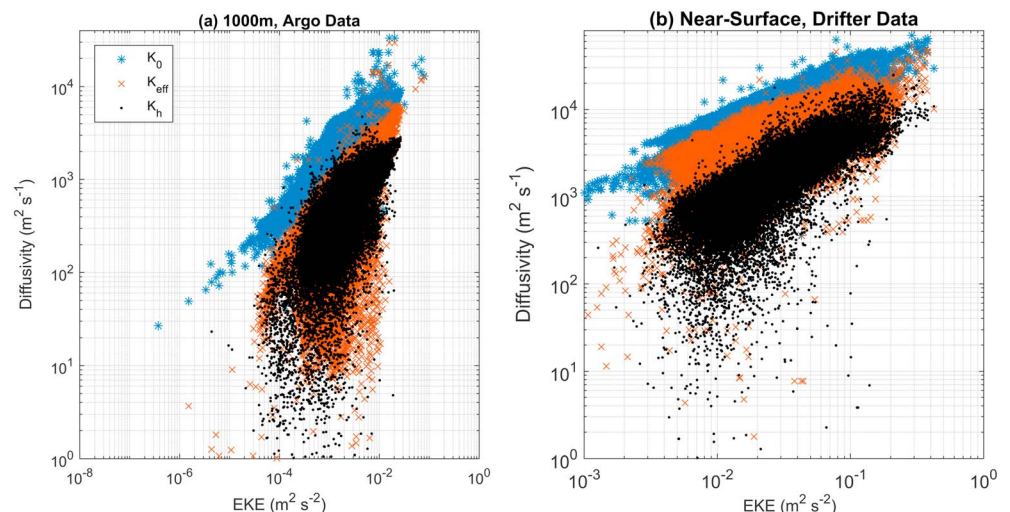


**Figure 8.** Scatter plot of diffusivity as a function of EKE for (a) Argo and (b) drifter observations ( $K_h$ , black); theoretical results with no suppression ( $K_0$ , blue) and theoretical results with suppression ( $K_{\text{eff}}$ , orange).

900–4,900  $\text{m}^2/\text{s}$ . The observed spatial patterns align well with the EKE, showing larger magnitudes in the boundary currents and the Antarctic Circumpolar Current and smaller magnitude on the eastern side of the gyre. These estimates of diffusivity were obtained using a two-particle analysis and are representative of the stirring that acts across the mean flow. The associated spatial scales are on the order of a few hundred kilometers, and thus, our diffusivity estimates are representative of the diffusivity due to the largest eddies that stir fluid by uncorrelated velocities.

A simple parameterization of diffusivity based on observed eddy size and eddy energy performed poorly, giving diffusivity estimates that were about 3–3.5 times greater than the observed diffusivities. Comparison to a diffusivity parameterization based on mixing length suppression by a mean flow (Ferrari & Nikurashin, 2010) showed more promise, with the parameterized estimates being only about 1.5–2 times greater than the observed diffusivities, and capturing the observed patterns in the midlatitude and high latitude to a reasonable degree. This suggests that minor modifications to the current parameterizations might be required. Neither of the parameterizations showed much promise near the equator, suggesting that more theoretical work needs to be done to explain the observed patterns of eddy diffusivity.

A comparison of our diffusivity estimates against prior observational estimates showed good agreement, so long as the idiosyncrasies of the various methodologies are taken into account. The spatial patterns of our estimates agree remarkably well with global maps of eddy diffusivity that were estimated using the Argo hydrography (Cole et al., 2015) in the midlatitude and high latitude, albeit there was a factor of  $\sim 2$  disagreement in magnitude. Our estimates did not show a good agreement near the equator, with our diffusivities being significantly smaller. Comparison of our near-surface results with other studies using tracers advected in SSH fields (Abernathy & Marshall, 2013) or surface drifters (Zhurbas et al., 2014) demonstrated reasonable agreement in both structure and magnitude, with dissimilarities near the equator. Similarly, our ocean-interior results were consistent with a number of prior regional studies (Table 1).

This work supports the hypothesis of Roach et al. (2016) that Argo float trajectories can be used to get reasonable estimates of horizontal stirring, as the errors associated with the vertical profiling of the Argo float are of the same order as the statistical errors due to limited sampling, opening another avenue for using Argo data. As the Argo sampling is increased, and improvements in technology leads to quicker profiling and less time spent at the surface, the uncertainty on the estimates presented in this study should reduce. This study points at the need to increase Argo float profiling in the eastern Pacific Ocean, where poor sampling by Argo floats produces larger uncertainties in the estimates of this study. In the future, granting that the Argo program is continued and improved, it should become possible to examine the temporal variability of the large-scale global eddy diffusivity, associated with seasonality and low-frequency variability.

## Acknowledgments

Funding for this research was provided by NSF OCE 1231803, NSF OCE 0622670, and NSF OCE 0822075. We wish to thank S. Cole for making her mixing data set publically available and for a number of useful comments and suggestions during the review process. We also wish to thank an anonymous reviewer for comments that helped to improve the paper. Argo and surface drifter mixing fields are available at [https://github.com/croachutas/Isopycnal\\_Diffusivity](https://github.com/croachutas/Isopycnal_Diffusivity). We used data collected and made freely available by the International Argo Program and the national programs that contribute to it. (<http://www.argo.ucsd.edu>, <http://argo.jcommops.org>). The Argo Program is part of the Global Ocean Observing System. <http://doi.org/10.17882/42182>.

## References

- Abernathy, R. P., & Marshall, J. (2013). Global surface eddy diffusivities derived from satellite altimetry. *Journal of Geophysical Research: Oceans*, 118, 901–916. <https://doi.org/10.1002/jgrc.20066>
- Abernathy, R. P., & Wortham, C. (2015). Phase speed cross spectra of eddy heat fluxes in the eastern Pacific. *Journal of Physical Oceanography*, 45(5), 1285–1301. <https://doi.org/10.1175/JPO-D-14-0160.1>
- Armi, L., & Stommel, H. (1983). Four views of a portion of the North Atlantic Subtropical Gyre. *Journal of Physical Oceanography*, 13(5), 828–857. [https://doi.org/10.1175/1520-0485\(1983\)013<0828:fvoapo>2.0.co;2](https://doi.org/10.1175/1520-0485(1983)013<0828:fvoapo>2.0.co;2)
- Argo (2000). Argo float data and metadata from Global Data Assembly Centre (Argo GDAC). SEANO. <http://doi.org/10.17882/42182>
- Balwada, D., Speer, K. G., LaCasce, J. H., Owens, W. B., Marshall, J., & Ferrari, R. (2016). Circulation and stirring in the Southeast Pacific Ocean and the Scotia Sea sectors of the Antarctic Circumpolar Current. *Journal of Physical Oceanography*, 46(7), 2005–2027. <https://doi.org/10.1175/JPO-D-15-0207.1>
- Bates, M., Tulloch, R., Marshall, J., & Ferrari, R. (2014). Rationalizing the spatial distribution of mesoscale eddy diffusivity in terms of mixing length theory. *Journal of Physical Oceanography*, 44(6), 1523–1540. <https://doi.org/10.1175/jpo-d-13-0130.1>
- Bolster, D., Dentz, M., & Le Borgne, T. (2011). Hypermixing in linear shear flow. *Water Resources Research*, 47, W09602. <https://doi.org/10.1029/2011WR010737>
- Chelton, D. B., Schlax, M. G., & Samelson, R. M. (2011). Global observations of nonlinear mesoscale eddies. *Progress in Oceanography*, 91(2), 167–216. <https://doi.org/10.1016/j.pocan.2011.01.002>
- Chiswell, S. M. (2013). Lagrangian time scales and eddy diffusivity at 1000 m compared to the surface in the South Pacific and Indian Oceans. *Journal of Physical Oceanography*, 43(12), 2718–2732. <https://doi.org/10.1175/JPO-D-13-044.1>
- Cole, S. T., Wortham, C., Kunze, E., & Owens, W. B. (2015). Eddy stirring and horizontal diffusivity from Argo float observations: Geographic and depth variability. *Geophysical Research Letters*, 42, 3989–3997. <https://doi.org/10.1002/2015GL063827>
- Cole, S. T., Wortham, C., Kunze, E., & Owens, W. B. (2018). Eddy diffusivity from Argo temperature and salinity profiles. doi: <https://doi.org/10.1575/1912/10220>. [Retrieved from <https://hdl.handle.net/1912/10220>]
- Davis, R. E. (1991). Observing the general circulation with floats. *Deep Sea Research Part A. Oceanographic Research Papers*, 38, S531–S571. [https://doi.org/10.1016/S0198-0149\(12\)80023-9](https://doi.org/10.1016/S0198-0149(12)80023-9)

- Davis, R. E., Sherman, J. T., & Dufour, J. (2001). Profiling ALACEs and other advances in autonomous subsurface floats. *Journal of Atmospheric and Oceanic Technology*, 18(6), 982–993. [https://doi.org/10.1175/1520-0426\(2001\)018<0982:paaoi>2.0.co;2](https://doi.org/10.1175/1520-0426(2001)018<0982:paaoi>2.0.co;2)
- Faure, V., & Speer, K. (2012). Deep circulation in the eastern South Pacific Ocean. *Journal of Marine Research*, 70(5), 748–778. <https://doi.org/10.1357/002224012806290714>
- Ferrari, R., & Nikurashin, M. (2010). Suppression of eddy diffusivity across jets in the Southern Ocean. *Journal of Physical Oceanography*, 40(7), 1501–1519. <https://doi.org/10.1175/2010JPO4278.1>
- Fox-Kemper, B., Lumpkin, R., & Bryan, F. O. (2013). Chapter 8 - Lateral Transport in the Ocean Interior. In G. Siedler, S. M. Griffies, J. Gould, & J. A. Church (Eds.), *Ocean circulation and climate: a 21st century perspective* (Vol. 103, pp. 185–209). Oxford: Academic Press.
- Fu, L. L. (2009). Pattern and velocity of propagation of the global ocean eddy variability. *Journal of Geophysical Research*, 114, C11017. <https://doi.org/10.1029/2009JC005349>
- Gent, P. R., & McWilliams, J. C. (1990). Isopycnal mixing in ocean circulation models. *Journal of Physical Oceanography*, 20(1), 150–155. [https://doi.org/10.1175/1520-0485\(1990\)020<0150:IMOCM>2.0.CO;2](https://doi.org/10.1175/1520-0485(1990)020<0150:IMOCM>2.0.CO;2)
- Gille, S. T. (2003). Float observations of the Southern Ocean. Part II: Eddy fluxes. *Journal of Physical Oceanography*, 33(6), 1182–1196. [https://doi.org/10.1175/1520-0485\(2003\)033<1182:Footso>2.0.co;2](https://doi.org/10.1175/1520-0485(2003)033<1182:Footso>2.0.co;2)
- Gnanadesikan, A., Bianchi, D., & Pradal, M. A. (2013). Critical role for mesoscale eddy diffusion in supplying oxygen to hypoxic ocean waters. *Geophysical Research Letters*, 40, 5194–5198. <https://doi.org/10.1002/grl.50998>
- Gray, A. R., & Riser, S. C. (2014). A global analysis of sverdrup balance using absolute geostrophic velocities from Argo. *Journal of Physical Oceanography*, 44(4), 1213–1229. <https://doi.org/10.1175/jpo-d-12-0206.1>
- Griesel, A., Gille, S. T., Sprintall, J., McClean, J. L., LaCasce, J. H., & Maltrud, M. E. (2010). Isopycnal diffusivities in the Antarctic Circumpolar Current inferred from Lagrangian floats in an eddying model. *Journal of Geophysical Research*, 115, C06006. <https://doi.org/10.1029/2009JC005821>
- Groeskamp, S., Sloyan, B. M., Zika, J. D., & McDougall, T. J. (2017). Mixing inferred from an ocean climatology and surface fluxes. *Journal of Physical Oceanography*, 47(3), 667–687. <https://doi.org/10.1175/jpo-d-16-0125.1>
- Hastenrath, S., & Lamb, P. (1978). On the dynamics and climatology of surface flow over the equatorial oceans. *Tellus*, 30(5), 436–448. <https://doi.org/10.1111/j.2153-3490.1978.tb00859.x>
- Katsumata, K., & Yoshinari, H. (2010). Uncertainties in global mapping of Argo drift data at the parking level. *Journal of Oceanography*, 66(4), 553–569. <https://doi.org/10.1007/s10872-010-0046-4>
- Klocker, A., & Abernathey, R. (2014). Global patterns of mesoscale eddy properties and diffusivities. *Journal of Physical Oceanography*, 44(3), 1030–1046. <https://doi.org/10.1175/jpo-d-13-0159.1>
- Klocker, A., Ferrari, R., LaCasce, J. H., & Merrifield, S. T. (2012). Reconciling float-based and tracer-based estimates of eddy. *Journal of Marine Research*, 70(4), 569–602. <https://doi.org/10.1357/002224012805262743>
- LaCasce, J. H. (2008). Statistics from Lagrangian observations. *Progress in Oceanography*, 77(1), 1–29. <https://doi.org/10.1016/j.pocean.2008.02.002>
- LaCasce, J. H., & Bower, A. (2000). Relative dispersion in the subsurface North Atlantic. *Journal of Marine Research*, 58(6), 863–894. <https://doi.org/10.1357/002224000763485737>
- LaCasce, J. H., Ferrari, R., Marshall, J., Tulloch, R., Balwada, D., & Speer, K. (2014). Float-derived isopycnal diffusivities in the DIMES experiment. *Journal of Physical Oceanography*, 44(2), 764–780. <https://doi.org/10.1175/JPO-D-13-0175.1>
- Lebedev, K. V., Yoshinari, H., Maximenko, N. A., & Hacker, P. W. (2007). YoMaHa'07: Velocity data assessed from trajectories of Argo floats at parking level and at the sea surface. [Retrieved from <http://apdr.csoest.hawaii.edu/projects/yomaha/yomaha07/YoMaHa070612.pdf>.]
- Ledwell, J. R., Watson, A. J., & Law, C. S. (1998). Mixing of a tracer in the pycnocline. *Journal of Geophysical Research*, 103, 21,499–21,529. <https://doi.org/10.1029/98JC01738>
- Lumpkin, R., Grodsky, S. A., Centurioni, L., Rio, M.-H., Carton, J. A., & Lee, D. (2013). Removing spurious low-frequency variability in drifter velocities. *Journal of Atmospheric and Oceanic Technology*, 30(2), 353–360. <https://doi.org/10.1175/jtech-d-12-00139.1>
- Marshall, J., & Speer, K. (2012). Closure of the meridional overturning circulation through Southern Ocean upwelling. *Nature Geoscience*, 5(3), 171–180. <https://doi.org/10.1038/ngeo1391>
- Meredith, M. P., Naveira Garabato, A. C., Hogg, A. M., & Farneti, R. (2011). Sensitivity of the overturning circulation in the Southern Ocean to decadal changes in wind forcing. *Journal of Climate*, 25(1), 99–110. <https://doi.org/10.1175/2011JCLI4204.1>
- Middleton, J. F. (1985). Drifter spectra and diffusivities. *Journal of Marine Research*, 43(1), 37–55. <https://doi.org/10.1357/002224085788437334>
- Naveira Garabato, A. C., Ferrari, R., & Polzin, K. L. (2011). Eddy stirring in the Southern Ocean. *Journal of Geophysical Research*, 116, C09019. <https://doi.org/10.1029/2010JC006818>
- Naveira-Garabato, A. C., Stevens, D. P., Watson, A. J., & Roether, W. (2007). Short-circuiting of the overturning circulation in the Antarctic circumpolar current. *Nature*, 447(7141), 194–197. [Retrieved from [http://www.nature.com/nature/journal/v447/n7141/supinfo/nature05832\\_s1.html](http://www.nature.com/nature/journal/v447/n7141/supinfo/nature05832_s1.html).]
- Ollitrault, M., Gabillet, C., & De Verdiere, A. C. (2005). Open ocean regimes of relative dispersion. *Journal of Fluid Mechanics*, 533, 381–407. <https://doi.org/10.1017/S0022112005004556>
- Roach, C. J., Balwada, D., & Speer, K. (2016). Horizontal mixing in the Southern Ocean from Argo float trajectories. *Journal of Geophysical Research: Oceans*, 121, 5570–5586. <https://doi.org/10.1002/2015JC011440>
- Rypina, I. I., Brown, M., Beron-Vera, F., Koçak, H., Olascoaga, M., & Udovychdenkov, I. (2007). Robust transport barriers resulting from strong Kolmogorov-Arnold-Moser stability. *Physical Review Letters*, 98(10), 104102. <https://doi.org/10.1103/PhysRevLett.98.104102>
- Rypina, I. I., Kamenkovich, I., Berloff, P., & Pratt, L. J. (2012). Eddy-induced particle dispersion in the near-surface North Atlantic. *Journal of Physical Oceanography*, 42(12), 2206–2228. <https://doi.org/10.1175/JPO-D-11-0191.1>
- Sallee, J.-B., Speer, K., & Rintoul, S. (2011). Mean-flow and topographic control on surface eddy-mixing in the Southern Ocean. *Journal of Marine Research*, 69(4), 753–777. <https://doi.org/10.1357/002224011799849408>
- Smith, K. S. (2007). The geography of linear baroclinic instability in Earth's oceans. *Journal of Marine Research*, 65(5), 655–683. <https://doi.org/10.1357/002224007783649484>
- Spall, M. A., Richardson, P. L., & Price, J. (1993). Advection and eddy mixing in the Mediterranean salt tongue. *Journal of Marine Research*, 51(4), 797–818. <https://doi.org/10.1357/0022240933223882>
- Speer, K., Rintoul, S. R., & Sloyan, B. (2000). The diabatic deacon cell. *Journal of Physical Oceanography*, 30(12), 3212–3222. [https://doi.org/10.1175/1520-0485\(2000\)030<3212:TDDC>2.0.CO;2](https://doi.org/10.1175/1520-0485(2000)030<3212:TDDC>2.0.CO;2)
- Srinivasan, K., & Young, W. (2014). Reynolds stress and eddy diffusivity of  $\beta$ -plane shear flows. *Journal of the Atmospheric Sciences*, 71(6), 2169–2185. <https://doi.org/10.1175/JAS-D-13-0246.1>

- Taylor, G. (1921). Diffusion by continuous movements. *Proceedings of the London Mathematical Society*, 20, 196–211.
- Treguier, A.-M., Held, I., & Larichev, V. (1997). Parameterization of quasigeostrophic eddies in primitive equation ocean models. *Journal of Physical Oceanography*, 27(4), 567–580. [https://doi.org/10.1175/1520-0485\(1997\)027<0567:POQEIP>2.0.CO;2](https://doi.org/10.1175/1520-0485(1997)027<0567:POQEIP>2.0.CO;2)
- Tulloch, R., Ferrari, R., Jahn, O., Klocker, A., LaCasce, J., Ledwell, J. R., et al. (2014). Direct estimate of lateral Eddy diffusivity upstream of drake passage. *Journal of Physical Oceanography*, 44(10), 2593–2616. <https://doi.org/10.1175/JPO-D-13-0120.1>
- Tulloch, R., Marshall, J., Hill, C., & Smith, K. S. (2011). Scales, growth rates, and spectral fluxes of baroclinic instability in the ocean. *Journal of Physical Oceanography*, 41(6), 1057–1076. <https://doi.org/10.1175/2011JPO4404.1>
- Visbeck, M., Marshall, J., Haine, T., & Spall, M. (1997). Specification of eddy transfer coefficients in coarse-resolution ocean circulation models. *Journal of Physical Oceanography*, 27(3), 381–402. [https://doi.org/10.1175/1520-0485\(1997\)027<0381:SOETCI>2.0.CO;2](https://doi.org/10.1175/1520-0485(1997)027<0381:SOETCI>2.0.CO;2)
- Wilk, M. B., & Gnanadesikan, R. (1968). Probability plotting methods for the analysis of data. *Biometrika*, 55(1), 1–17. <https://doi.org/10.2307/2334448>
- Young, W. a., & Jones, S. (1991). Shear dispersion. *Physics of Fluids A: Fluid Dynamics*, 3(5), 1087–1101. <https://doi.org/10.1063/1.858090>
- Zheng, Q., Yan, X.-H., Liu, W. T., Tang, W., & Kurz, D. (1997). Seasonal and interannual variability of atmospheric convergence zones in the tropical Pacific observed with ERS-1 scatterometer. *Geophysical Research Letters*, 24, 261–263. <https://doi.org/10.1029/97GL00033>
- Zhurbas, V., Lyzhkov, D., & Kuzmina, N. (2014). Drifter-derived estimates of lateral eddy diffusivity in the world ocean with emphasis on the Indian Ocean and problems of parameterisation. *Deep Sea Research Part I: Oceanographic Research Papers*, 83, 1–11. <https://doi.org/10.1016/j.dsr.2013.09.001>
- Zhurbas, V., & Oh, I. S. (2003). Lateral diffusivity and Lagrangian scales in the Pacific Ocean as derived from drifter data. *Journal of Geophysical Research*, 108(C5), 3141. <https://doi.org/10.1029/2002JC001596>
- Zika, J. D., McDougall, T. J., & Sloyan, B. M. (2010). Weak mixing in the eastern North Atlantic: An application of the tracer-contour inverse method. *Journal of Physical Oceanography*, 40(8), 1881–1893. <https://doi.org/10.1175/2010jpo4360.1>
- Zika, J. D., Sloyan, B. M., & McDougall, T. J. (2009). Diagnosing the Southern Ocean overturning from tracer fields. *Journal of Physical Oceanography*, 39(11), 2926–2940. <https://doi.org/10.1175/2009jpo4052.1>